



## Stabilization of Platinum Anode Catalyst in a $\text{H}_2\text{S}$ - $\text{O}_2$ Solid Oxide Fuel Cell with an Intermediate $\text{TiO}_2$ Layer

P. He, M. Liu, J. L. Luo,<sup>\*,z</sup> A. R. Sanger, and K. T. Chuang

Department of Chemical and Materials Engineering, University of Alberta, Edmonton, Alberta T6G 2G6, Canada

The performance of supported platinum as an anode catalyst in a hydrogen sulfide solid oxide fuel cell with yttria-stabilized zirconia (YSZ) as the electrolyte has been examined in the temperature range of 700–900°C. The highest current density achieved at 800°C was 100 mA/cm<sup>2</sup> and the highest power density was 15.4 mW/cm<sup>2</sup>, when operated with 5%  $\text{H}_2\text{S}$  feed. Increasing the concentration of  $\text{H}_2\text{S}$  in the anode feed did not improve the performance of the cell, due to corrosion of the platinum anode; the reversible formation and decomposition of PtS on the platinum-YSZ interface led to instability of the electrochemical interface of the Pt catalyst with the YSZ electrolyte. The membrane structure and performance were both stabilized by interposing a thin layer of  $\text{TiO}_2$  between the Pt anode and YSZ electrolyte. The stabilized open-circuit voltage value depended on flow rates of the anode and cathode feeding gases. This behavior is attributed to the crossover of reactants, which change the partial pressures of product  $\text{SO}_2$  and  $\text{H}_2\text{O}$ .

© 2002 The Electrochemical Society. [DOI: 10.1149/1.1479156] All rights reserved.

Manuscript submitted November 13, 2000; revised manuscript received December 11, 2001. Available electronically May 9, 2002.

It has long been recognized that hydrogen sulfide ( $\text{H}_2\text{S}$ ) is a potentially valuable fuel for a fuel cell.  $\text{H}_2\text{S}$  has a high heating value. The electrochemical reaction products,  $\text{SO}_2$  or elemental sulfur, are important commodities. However,  $\text{H}_2\text{S}$  gas is both noxious and a poison to  $\text{H}_2$ - $\text{O}_2$  fuel cell anode catalysts, which made examination of  $\text{H}_2\text{S}$  in a fuel cell difficult or impractical until the late 1980s.<sup>1–3</sup> Pujare *et al.*<sup>1,2</sup> investigated high-temperature (900°C)  $\text{H}_2\text{S}$ - $\text{O}_2$  solid oxide fuel cells (SOFC) using yttria (8 wt %) or calcia (5 wt %) stabilized zirconia as the electrolyte. These oxides were found to tolerate a high level of  $\text{H}_2\text{S}$  as feed. This work showed the feasibility of using  $\text{H}_2\text{S}$  in high-temperature SOFC. A series of thiospinel anodes also was examined, and a current of *ca.* 16 mA/cm<sup>2</sup> was achieved at 500 mV anodic overpotential using  $\text{CuFe}_2\text{S}_4$  as the anode catalyst.

A major effort has been made by Winnick *et al.*<sup>4–7</sup> to improve the efficiency of  $\text{H}_2\text{S}$ - $\text{O}_2$  fuel cells and to develop membrane assemblies active at reduced operating temperatures. Various types of ionic conductors and anode materials have been prepared and tested. It was found that the ionic conducting materials strontium cerate ( $\text{SrCe}_{0.95}\text{Yb}_{0.05}\text{O}_3$ ) and barium cerate ( $\text{BaCe}_{0.95}\text{Yb}_{0.05}\text{O}_3$ ) were not stable in a  $\text{H}_2\text{S}$  atmosphere. The conducting cerates were converted to nonconductive sulfates ( $\text{SrSO}_4$  and  $\text{BaSO}_4$ ). Doped ceria exhibited higher conductivity than yttria-stabilized zirconia (YSZ). However, the electronic conductivity of ceria in a reducing atmosphere results in reduced cell performance.<sup>5,8</sup> The anode materials used in these studies included Pt,  $\text{WS}_2$ ,  $\text{CoS}_2$ , and Li/Co sulfide. The conductivities of  $\text{WS}_2$  and Li/Co sulfide were shown to be more stable than that of  $\text{CoS}_2$ . However, in each case the conductivity decayed over time with exposure to  $\text{H}_2\text{S}$ . The best output reported to date for a SOFC  $\text{H}_2\text{S}$  fuel cell is 400 mW/cm<sup>2</sup> power density, attained at 770°C using Li/Co sulfide anode material and a Siemens Westinghouse YSZ electrolyte/cathode assembly.<sup>7</sup>

Due to its stability and catalytic activity, platinum is commonly used as anode material and/or current collectors in  $\text{H}_2\text{S}$  fuel cells. In previous work by this group, a low-temperature proton-conducting  $\text{H}_2\text{S}$  fuel cell has been developed.<sup>9</sup> A carbon-supported platinum anode was shown to be an effective catalyst in the  $\text{H}_2\text{S}$  fuel cell. However, the Pt/C anode used in the low temperature fuel cell was physically unstable. The performance and stability of supported platinum anode catalysts under  $\text{H}_2\text{S}$  atmosphere at high temperatures has not been systematically investigated. In this report, the

stability of platinum anodes in a high temperature  $\text{H}_2\text{S}$  fuel cell are described. We show that applying a thin (submicrometer) layer of titania between the platinum anode and YSZ electrolyte improves the stability of the platinum anode. We report the performance and impedance of the cell using  $\text{H}_2\text{S}$  as fuel. The X-ray diffraction (XRD) structure of the solid electrolyte and platinum anode following the operation of each membrane in a  $\text{H}_2\text{S}$  fuel cell are described. The role of the titania layer is discussed.

### Experimental

**Equipment.**—A schematic diagram of the experimental  $\text{H}_2\text{S}$  fuel cell with planar cell geometry is given in Fig. 1. The anodic and cathodic chambers were constructed using mullite or alumina tubes. The electrode-electrolyte assembly was supported in a Pyrex holder situated between the two chambers. Aremco ceramic adhesive no. 503 was found to be effective and stable as a high-temperature sealant in the  $\text{H}_2\text{S}$ - $\text{O}_2$  fuel cell. Either 5%  $\text{H}_2\text{S}$  fuel gas (balance with nitrogen) or pure  $\text{H}_2\text{S}$  was fed into the anode compartment from the inner tube. Tailing gases were withdrawn from an outlet on the outer tube of the anode compartment. The two tubes were fastened together at a distant end located outside the oven containing the electrode-electrolyte assembly compartment. The cathode compartment was similar in structure to the anode compartment.

**Membrane preparation.**—Tape-casted 8 mol % yttria-stabilized zirconia (YSZ) (Marktech International, Inc.) was used as the electrolyte. The wafers of electrolyte had a thickness of 0.2 mm and a diameter of 25.4 mm. Platinum electrodes for both cathode and anode were prepared by screen printing platinum paste (Heraeus CL11-5100) onto the corresponding YSZ wafer surfaces. The wafer and platinum electrodes were gradually heated to 1050°C and held at that temperature for 30 min to remove the organics in the paste

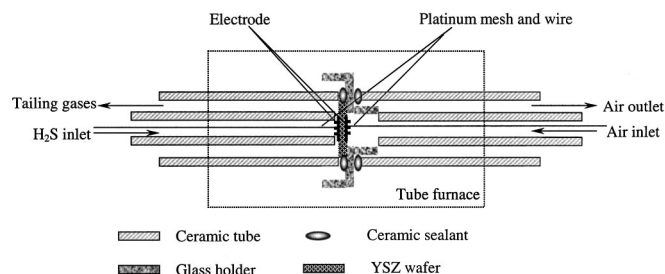


Figure 1. Configuration of  $\text{H}_2\text{S}$  fuel cell.

\* Electrochemical Society Active Member.

<sup>z</sup> E-mail: jingli.luo@ualberta.ca

and to increase adhesion to YSZ. The operating area of each electrode was approximately 1 cm<sup>2</sup>. Platinum meshes in close contact with the anode and cathode were used as current collectors.

**TiO<sub>2</sub>/YSZ wafer.**—A titania interlayer was applied to the anode surface of the YSZ wafer using the sol-gel and paste painting techniques, before depositing the Pt anode. Titania sol was made as described elsewhere<sup>10</sup> and spin-coated onto one surface of the YSZ wafer. The TiO<sub>2</sub>/YSZ wafer was fired in air at a heating rate of 3°C/min, and then held at 900°C for 2 h. A submicrometer TiO<sub>2</sub> layer was formed at the YSZ surface and had a shiny flaxen appearance when the interlayer was made by the sol-gel technique. The thickness of TiO<sub>2</sub> layer made by pasting was *ca.* 0.5 μm. The TiO<sub>2</sub> in this layer was shown by XRD to have a rutile structure. The firing temperature of the TiO<sub>2</sub> layer was maintained below 1000°C to minimize penetration of Ti ions into YSZ,<sup>11</sup> as is described below.

**Electrical measurements.**—The open-circuit voltage (OCV) of the fuel cell was monitored using a Keithley 199 digital multimeter. Potentiodynamic current-potential measurements were conducted using a Pine AFRED5 potentiostat in conjunction with a Virtual-Bench data acquisition system to acquire data automatically. Cell impedance analysis was carried out using a Gamry CMS 300/100 impedance measurement system and a Stanford SR810 DSP lock-in amplifier.

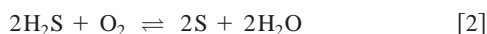
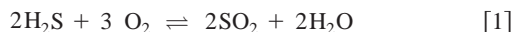
**Characterization of solids.**—Scanning electron microscopy (SEM) and energy dispersive X-ray (EDX) measurements were conducted using a Hitachi model S-2700 scanning electron microscope and PGT Imix system with a Prism IG. XRD spectra were obtained using a Rigaku Rotaflex X-ray diffractometer.

**Materials.**—Anode feed gases were hydrogen sulfide (CP grade) and 5% hydrogen sulfide (balance nitrogen) compressed gases (Praxair). Compressed air (Praxair) was used as the cathode feed.

**Analysis of feed and exit gas streams.**—The feed and exit gas stream were analyzed with a gas chromatograph (Hewlett Packard, model 5890), using a molecular sieve column at 130°C and a thermal conductivity detector (TCD) detector connected to an HP3396 series II integrator.

## Results and Discussion

**Performance and stability of Pt anode in an H<sub>2</sub>S fuel cell.**—Figure 2 shows the relationship between cell voltage and power density to current density at temperatures of 750 and 800°C for the H<sub>2</sub>S-O<sub>2</sub> fuel cell having the arrangement of H<sub>2</sub>S (5%), Pt/YSZ (8% mol yttrium, 200 μm)/Pt, air. The maximum current and output power achieved using this system were 100 and 16 mW/cm<sup>2</sup> at 800°C, respectively. The voltage-current curves were not IR corrected. The resistance of the platinum leads and the contact resistance between Pt leads and electrodes was 2.0–4.5 Ω at the operating temperatures, the precise value depending on the individual experiment. The OCV was above 1.0 V at each temperature. This value was higher than the theoretical values for the oxidation of H<sub>2</sub>S to either SO<sub>2</sub> (Eq. 1) or elemental sulfur (Eq. 2) under standard conditions. The theoretical equilibrium voltages for the two reactions under standard condition are 0.757 and 0.741 V at 750°C, and 0.750 and 0.725 V at 800°C, respectively, based on thermodynamic data (HSC Chemistry, Version 1.12, equilibrium equations, Outokumpu Research)



In practice, the partial pressures of  $p_{\text{H}_2\text{O}}$  and  $p_{\text{SO}_2}$  during operation of the fuel cell are much lower than the values under standard conditions. For theoretical calculations, the partial pressures for  $p_{\text{H}_2\text{O}}$  and  $p_{\text{SO}_2}$  are both assumed to be 1 atm, while in our system the total

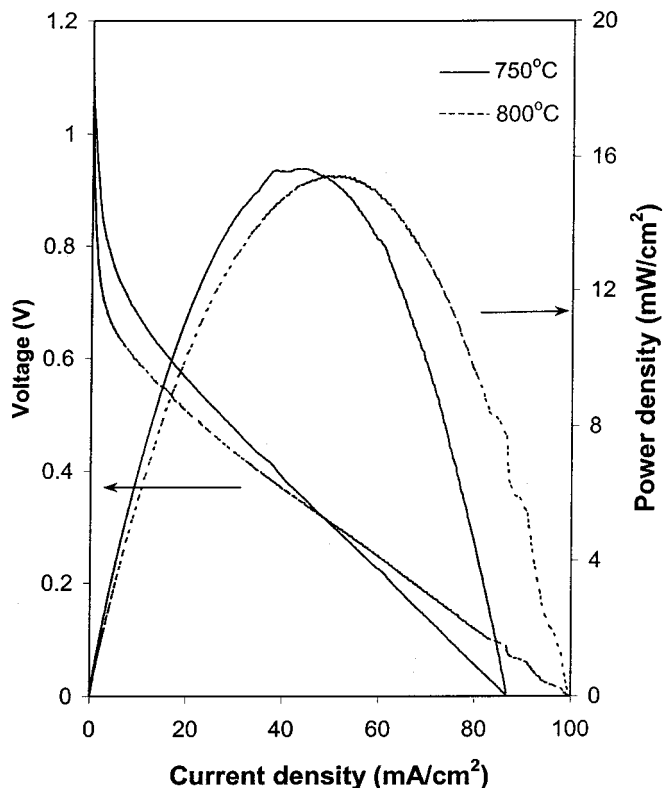


**Figure 2.** Current as a function of voltage and power curve of platinum anode in H<sub>2</sub>S fuel cell at 750 and 800°C. Fuel gas: 5% H<sub>2</sub>S.

pressure was 1 atm and the partial pressures of  $p_{\text{H}_2\text{O}}$  and  $p_{\text{SO}_2}$  were much lower than 1 atm. The concentration of SO<sub>2</sub> under open-circuit conditions is very small, and cannot be accurately quantified by gas chromatography (GC) because of the predominance of H<sub>2</sub>S in the exhaust stream. Consequently, the measured OCV value is higher than the voltages at the standard condition according to the following Nernst equation of the H<sub>2</sub>S-O<sub>2</sub> fuel cell

$$E_N = E^0 - \frac{RT}{nF} \ln \left( \frac{p_{\text{H}_2\text{O}} p_{\text{SO}_2}}{p_{\text{H}_2\text{S}} p_{\text{O}_2}^{3/2}} \right) \quad [3]$$

where  $E^0$  is the cell potential at standard condition,  $R$  and  $T$  are the gas constant and absolute temperature, respectively.  $F$  is the Faraday constant.  $p_i$  is the pressure of species  $i$ . Further, the possibility exists that there is concurrent partial thermal decomposition of H<sub>2</sub>S to hydrogen and elemental sulfur at the operating conditions. The presence of hydrogen at the anode would lead to a higher OCV value.<sup>7</sup>

The voltage-current behavior with H<sub>2</sub> as the fuel in the same cell construction (H<sub>2</sub>-O<sub>2</sub> fuel cell) was substantially similar to the H<sub>2</sub>S-O<sub>2</sub> fuel cell. The maximum current density in H<sub>2</sub>-O<sub>2</sub> fuel cell was almost the same as that in the fresh H<sub>2</sub>S-O<sub>2</sub> fuel cell. Thus the Pt electrode is an active anode for H<sub>2</sub>S-O<sub>2</sub> fuel cell. However, the voltage-current performance in the H<sub>2</sub>S-O<sub>2</sub> fuel cell was not stable over time. The current density decreased with time on stream. Concurrently, the cell resistance monitored using impedance spectroscopy increased. A high operating current of the H<sub>2</sub>S-O<sub>2</sub> fuel cell significantly accelerated the cell degradation. The current density decreased steadily over time at a rate depending on the voltage, until the Pt anode separated fully from the YSZ. This behavior was found to be due to the progressive detachment of the anode from the YSZ wafer.

The concentration of H<sub>2</sub>S in the feed also has a significant influence on cell performance. Pure H<sub>2</sub>S feed gave a reduced cell per-

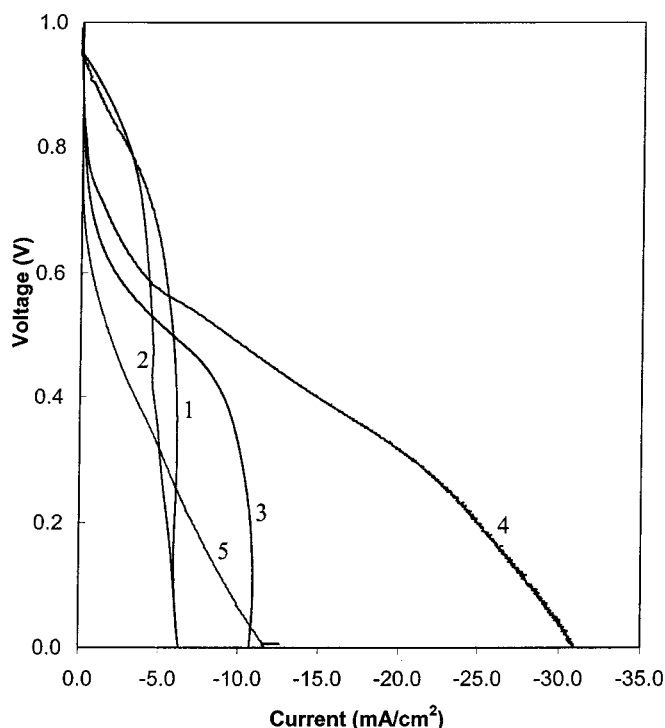


**Figure 3.** Current as a function of voltage at different temperature; 1, 700; 2, 750; 3, 800; 4, 850; and 5, 900; 100%  $\text{H}_2\text{S}$  fuel feed.

formance (current-voltage) when compared with the use of 5%  $\text{H}_2\text{S}$  feed. Figure 3 presents the current-voltage curves for pure  $\text{H}_2\text{S}$  feed at different temperatures. Clearly, the cell performance with pure  $\text{H}_2\text{S}$  feed is lower than that with 5%  $\text{H}_2\text{S}$  feed. In pure  $\text{H}_2\text{S}$  feed at 800°C the cell ceased to operate after about 5-6 h. In contrast, there was no significant decline in voltage-current performance over time using hydrogen as fuel.

From 700 to 850°C, the voltage-current performance of the  $\text{H}_2\text{S}$ - $\text{O}_2$  fuel cell improved with increasing temperature, although the OCV of the cell decreased. The curves (700-800°C, Fig. 3) show a precipitous decline in the high current density range, which is characteristic of mass-transport limitation. At 900°C, the voltage-current performance (curve 5, Fig. 3) dropped significantly. This decline was irreversible; the original performance could not be restored by reducing the temperature of operation.

The improvement of voltage-current performance with temperature in the  $\text{H}_2$ - $\text{O}_2$  fuel cell is normally ascribed to an increase in the electrochemical reaction rate and ionic conductivity of YSZ with temperature.<sup>12</sup> In the  $\text{H}_2\text{S}$ - $\text{O}_2$  fuel cell, the electrochemical reaction rate and ionic conductivity also increase with temperature,<sup>13,14</sup> and the activation energy of Reaction 1 decreases with increasing temperature. However, the fuel cell with 5%  $\text{H}_2\text{S}$  feed had a higher current density at each temperature, and no obvious mass-transport limitation was observed (Fig. 2). YSZ conductivity and the dependence of the reaction rate on temperature alone do not account for the observed lack of mass-transport limitation using 5%  $\text{H}_2\text{S}$  as feed. It is known that the platinum surface is readily converted to platinum sulfide (PtS) in a  $\text{H}_2\text{S}$  atmosphere. Forming a PtS layer on the platinum surface impedes the transport of the reactant gas onto the Pt surface and transport of products away from the active Pt sites. Thermodynamic calculations indicate that the equilibrium content of PtS exponentially decreases with increasing temperature (Fig. 4), due to thermal decomposition of PtS into sulfur vapor and platinum. Therefore, the PtS layer is reduced at elevated temperatures, and the limiting transportation current density increases with increasing temperature from 700 to 850°C, as shown in Fig. 3.

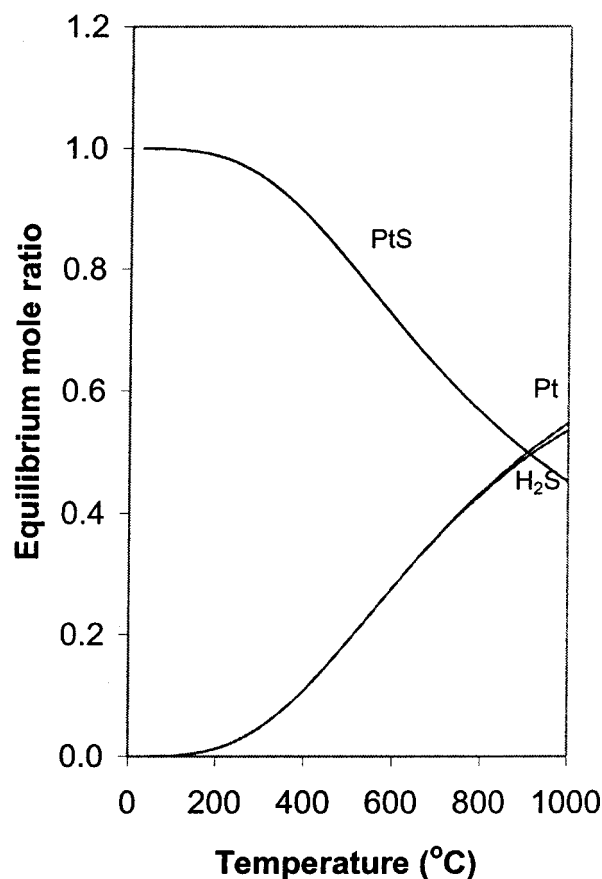


**Figure 4.** Equilibrium components in the system Pt/PtS/ $\text{H}_2\text{S}$  as a function of temperature. (HSC Chemistry, Version 1.12, equilibrium equations, Outokumpu Research.)

The cell OCV has been found to be related to the history of the anode. When the anode was first tested at 800°C, an initial cell OCV above 1.0 V was achieved, which then decreased with time on stream. However, when an anode had been used to acquire data at 700°C and the temperature was then increased to the higher temperature, it was found that an accumulation of PtS at the Pt/YSZ interface had fouled the Pt active sites, resulting in decreased cell OCV for that higher temperature.

Degradation of the Pt anode due to contamination in the  $\text{H}_2\text{S}$  stream is also demonstrated by the results shown in Fig. 5. All three measurements were conducted at 700°C. Curve 2 was recorded 5 h later than curve 1, during which the cell was exposed to pure  $\text{H}_2\text{S}$  feed and operated for measuring voltage-current curves several times. It can be seen that the maximum current density for the used cell is just one-tenth the value for the fresh cell. Curve 3 shows the voltage-current performance after switching the feed gases to both chambers from  $\text{H}_2\text{S}$  and air to  $\text{H}_2$ , and polarizing the electrode between 1.0 and -1.0 V vs.  $\text{H}^+/\text{H}_2$  electrode at 20 mV/s for one cycle. Voltage-current performance was partially regenerated when the catalyst surface was polarized in hydrogen atmosphere at 700°C. Polarization of the contaminated electrode in hydrogen partly cleans the platinum surface and restores the cell performance. After completion of the  $\text{H}_2\text{S}$ - $\text{O}_2$  fuel cell tests the Pt anode was easily peeled from the YSZ wafer. The XRD of the Pt anode showed that PtS had formed on the electrode (Fig. 6). On the YSZ surface, Pt, PtS, and YSZ were all present, but no new zirconia-based phase was detected on YSZ, which indicates that  $\text{H}_2\text{S}$  did not affect the cubic fluorite structure of YSZ during the experiment.

The poor voltage-current performance of the  $\text{H}_2\text{S}$ - $\text{O}_2$  fuel cell at 900°C (Fig. 3) is a result of the detachment of the Pt anode from the

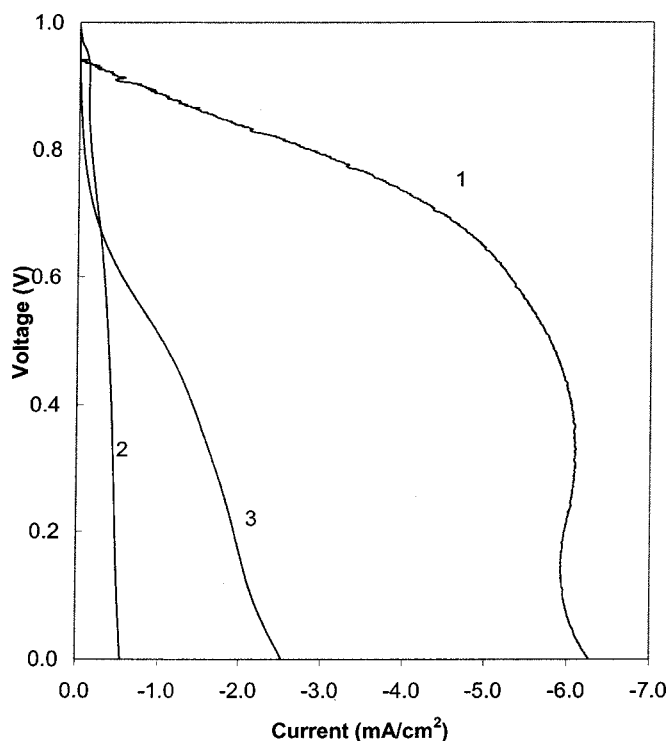


**Figure 5.** Current as a function of voltage for a  $\text{H}_2\text{S}$  fuel cell at  $700^\circ\text{C}$ . 100%  $\text{H}_2\text{S}$  feed. Curve 1: after 1 h operation; curve 2: after 6 h operation; curve 3: after polarization of the cell in  $\text{H}_2$  atmosphere.

YSZ wafer. Impedance tests revealed that the electronic resistance increased from  $2.5$  to  $15\ \Omega$  over time. After the experiment, it was found that the Pt anode had detached from the YSZ wafer. The anode detachment is ascribed to the formation of PtS in the Pt/YSZ interface during the electrochemical reaction process, during which the PtS changed the morphology of the electrochemical interface. At high temperatures, dynamic reversible formation and decomposition of PtS on the platinum surface in  $\text{H}_2\text{S}$  stream thereby caused instability of the Pt/YSZ interface. The rate of deterioration of the anode catalyst system depended on the operating current density. A high current density accelerated the mass transportation of  $\text{H}_2\text{S}$  toward the Pt/YSZ interface and formation of PtS, and hence accelerated detachment of the Pt anode from the YSZ. On the cathode side of the YSZ wafer, no detachment of the Pt cathode from the YSZ interface was detected. Thus the detachment of the anode was caused directly by the presence of  $\text{H}_2\text{S}$ . Although the effect is similar, the present phenomenon is unrelated to the morphological change of Ni particles in Ni-YSZ cermet anode in  $\text{H}_2$ - $\text{O}_2$  SOFC.<sup>15</sup>

When the cell was cooled down under a  $\text{N}_2$  atmosphere, it was found that the detached anode had adhered to the Pt mesh connector. The stability of the Pt-Pt connection is attributed to bonding of the Pt-Pt surface when sulfur in PtS was baked out from the adjacent surfaces of the connector and the anode at high temperature ( $700$  to  $900^\circ\text{C}$ ) under  $\text{N}_2$ . A fortuitous consequence is that, in this way, contact resistance between connector and electrode in a  $\text{H}_2\text{S}$  fuel cell is reduced due to the sequential exposure to  $\text{H}_2\text{S}$  atmosphere and baking in  $\text{N}_2$ . Impedance experiments revealed that the electronic resistance in the  $\text{H}_2\text{S}$  fuel cell had decreased slightly after treating in  $\text{H}_2\text{S}$  then baking in  $\text{N}_2$ , from  $2.8$  to  $2.2\ \Omega$ .

*Improvement of anode-YSZ stability by interposition of a  $\text{TiO}_2$  layer.*—The above experiment showed that the Pt/YSZ interface was unstable in a high-temperature  $\text{H}_2\text{S}$  environment. We have examined the interposition of an intermediate layer between the Pt anode and the YSZ wafer, with the objective of improving the bond-

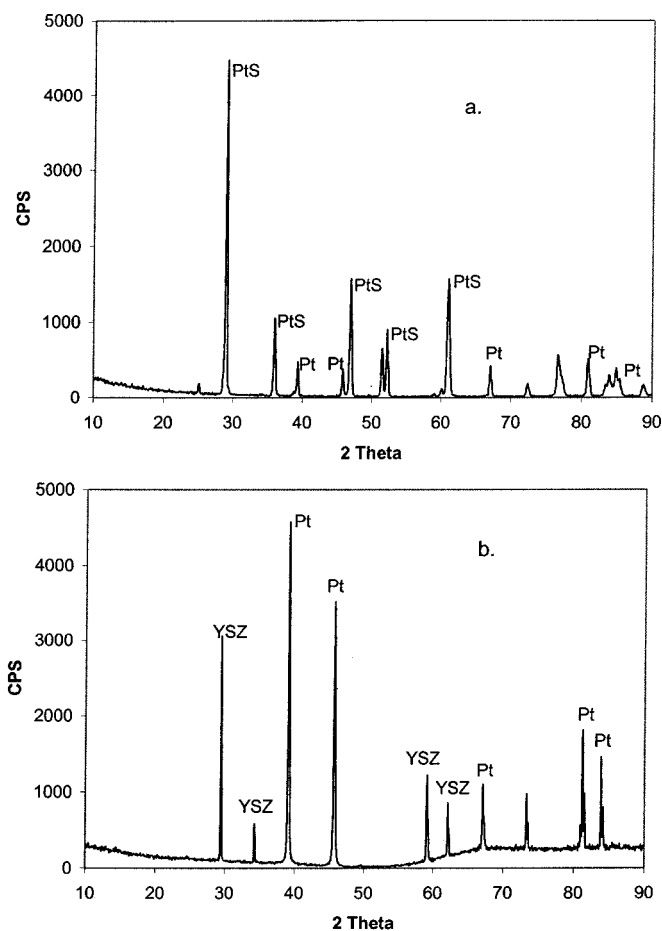


**Figure 6.** XRD spectra of Pt anode and YSZ surface after  $\text{H}_2\text{S}$  fuel cell test. (a) Disconnected Pt anode cooled down without passing  $\text{N}_2$ ; (b) anodic surface of YSZ after cooled down under  $\text{N}_2$ .

ing of the Pt anode and YSZ without compromising the activity of Pt, thereby improving the Pt anode stability in the  $\text{H}_2\text{S}$ - $\text{O}_2$  fuel cell. An ideal interposed bonding layer should be very thin and must be a good ionic and electronic conductor and stable in a  $\text{H}_2\text{S}$  environment. Titanium dioxide was selected, as it is a good catalyst for dissociation and oxidation of  $\text{H}_2\text{S}$  in the Claus process.<sup>16,17</sup>  $\text{TiO}_2$  is stable in the presence of  $\text{H}_2\text{S}$  to temperatures as high as  $950^\circ\text{C}$ , and has a very high electronic conductivity in reducing atmospheres.<sup>18-20</sup> Hydrogen spillover<sup>21,22</sup> at the interface of Pt/ $\text{TiO}_2$  enhances the dissociation reaction and the electronic conductivity. It has been suggested that titania is a potentially useful candidate as an anode cermet component for SOFCs.<sup>18</sup>

A submicrometer layer of  $\text{TiO}_2$  was applied to the anode side of the YSZ wafer using the sol-gel technique. Figure 7 shows the scanning electron microscopy (SEM) plot of a cross section of the  $\text{TiO}_2$ /YSZ interface. The wafer was embedded in epoxy for handling during the measurement. As the thermal expansion coefficients of YSZ and  $\text{TiO}_2$  are different, a large number of cracks formed in the  $\text{TiO}_2$  layer, as expected. The  $\text{TiO}_2$  layer is seen to be in the submicrometer range, *ca.*  $0.2$ - $0.5\ \mu\text{m}$ . The platinum anode was then applied using a screen printing process. The platinum was on the top of  $\text{TiO}_2$  layer and occupied the cracks in  $\text{TiO}_2$ , and was thereby anchored to the YSZ by  $\text{TiO}_2$  islands. Although the heat-treatment temperature of the titania layer was below  $900^\circ\text{C}$ ,  $\text{Ti(IV)}$  ions have been found to have diffused into the YSZ structure after lengthy operation (two weeks) at high temperatures. Figure 8 shows the EDX analysis for titanium at different depths below the anode sur-



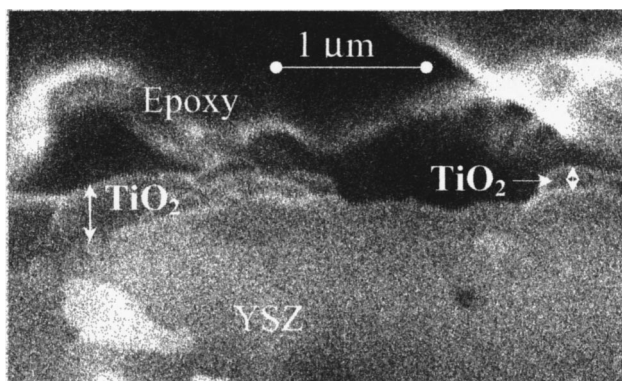


**Figure 7.** Cross-sectional SEM image of  $\text{TiO}_2$ /YSZ interface (sealed in epoxy).

face of the YSZ wafer. At locations  $1\ \mu\text{m}$  beneath the  $\text{TiO}_2$ /YSZ interface, 1.30 wt% titanium was detected. At  $3\ \mu\text{m}$  away from the interface, the content of Ti ions was below the resolution limit (*ca.* 0.1%) of the EDX instrumentation.

The OCV of the fuel cell,  $\text{H}_2\text{S}/\text{Pt}/\text{TiO}_2/\text{YSZ}/\text{Pt}$ , air, showed an unexpected dependence of performance on the flow rates of the anode and cathode streams. After the system had become stable, the OCV changed promptly with the change of flow rate ratio of air to

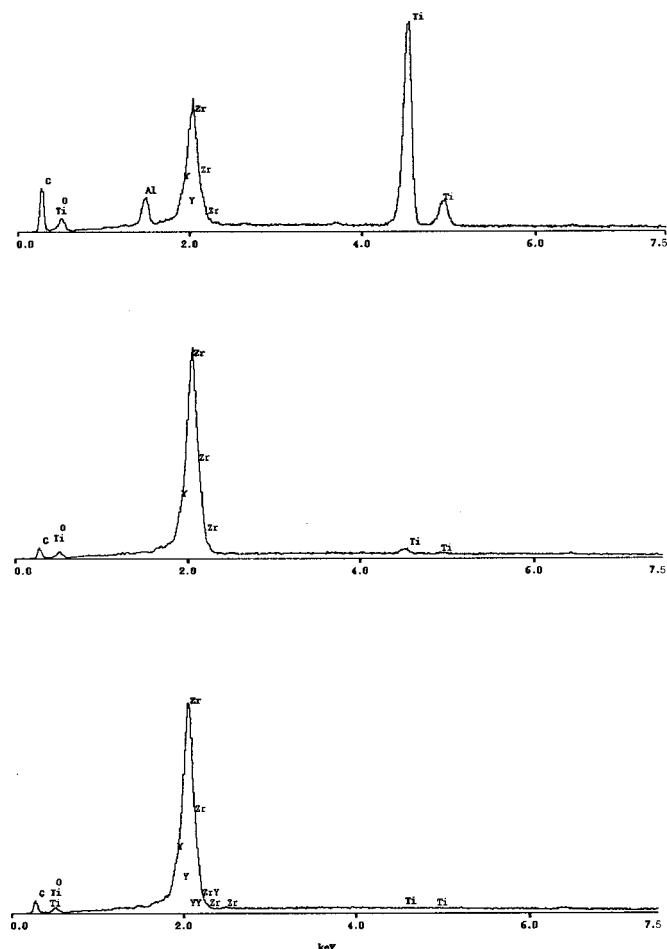


**Figure 8.** EDX measurement on the cross section of YSZ wafer after  $\text{H}_2\text{S}$  fuel cell testing, as a function of distance from the  $\text{TiO}_2$ /YSZ interface: (a, top)  $d = 0\ \mu\text{m}$ ; (b, center),  $d = 1\ \mu\text{m}$ ; (c, bottom),  $d = 3\ \mu\text{m}$ .

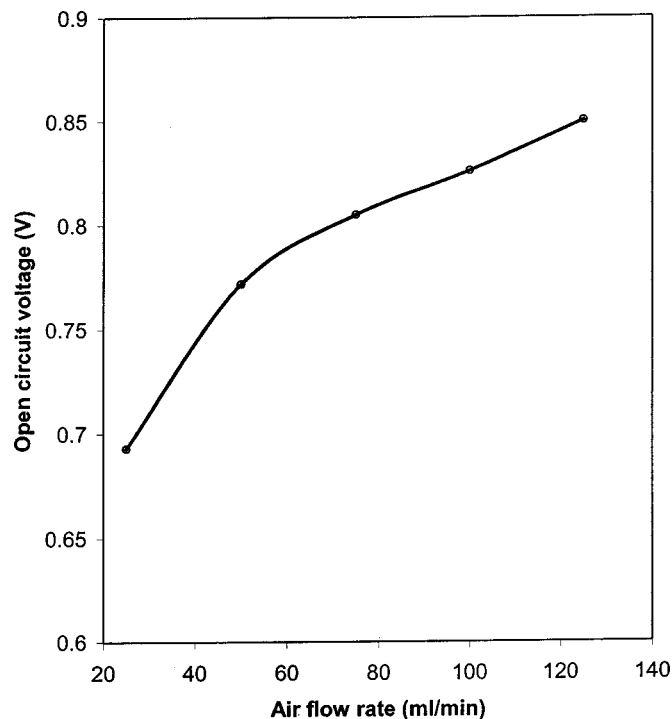


**Figure 9.** Open-circuit voltages of  $\text{H}_2\text{S}$  fuel cell with  $\text{TiO}_2$  layer as a function of air flow rate.  $\text{H}_2\text{S}$  (100%) flow rate: 15 mL/min;  $T$ :  $800^\circ\text{C}$ .

$\text{H}_2\text{S}$ . Figures 9 and 10 display the changes of OCV and voltage-current curves vs. air flow rate for a constant flow rate of  $\text{H}_2\text{S}$ . The higher the air flow rate, the higher the OCV value and better voltage-current performance. Likewise, when the air flow rate was constant and the  $\text{H}_2\text{S}$  flow rate was changed, a high  $\text{H}_2\text{S}$  flow rate gave a low OCV value. That is, the OCV increased with an increasing relative air flow rate and decreased with increasing relative  $\text{H}_2\text{S}$  flow rate. A reproducible OCV of 0.83 V was achieved for a flow rate ratio air,  $\text{H}_2\text{S} = 10:1$ . When the fuel gas was changed from  $\text{H}_2\text{S}$  to  $\text{H}_2$ , a similar relationship was observed, but with a lower OCV value compared to  $\text{H}_2\text{S}$  fuel at the same air-to-fuel flow rate ratios. The phenomenon can be attributed to the crossover of  $\text{H}_2\text{S}$  through the membrane. According to Eq. 3, an increase in water pressure and  $\text{SO}_2$  lead to a higher OCV. When the  $\text{H}_2\text{S}$  flow rate was high, the amount of the  $\text{H}_2\text{S}$  which crosses over the membrane would increase, and so the water pressure and probably  $\text{SO}_2$  at the cathode side would also increase due to reaction of  $\text{H}_2\text{S}$  with air at the cathode site, leading to a decrease of OCV. On the other hand, the OCV would increase when the air flow rate was increased because the high air flow rate would remove  $\text{H}_2\text{O}$  quickly. When the reactant gas was switched to  $\text{H}_2$ , the higher  $\text{H}_2$  crossover rate than  $\text{H}_2\text{S}$  gas resulted in a higher water pressure at the cathode, therefore a lower OCV value.

Performance as a function of temperature for the  $\text{H}_2\text{S}$  fuel cell using the wafer having the intermediate  $\text{TiO}_2$  anode layer (by the sol-gel method) is shown in Fig. 11. The performance of the cell improved with increasing operating temperature. The maximum output current of this cell was lower when compared to the cell without  $\text{TiO}_2$ . This decrease may be partially attributed to electrical loss in the internal cell, and also to changing of the electrochemical interface from  $\text{H}_2\text{S}/\text{Pt}/\text{YSZ}$  to  $\text{H}_2\text{S}/\text{Pt}/\text{TiO}_2/\text{YSZ}$ .

The electronic conductivity of  $\text{TiO}_2$  is very sensitive to reducing conditions, such as hydrogen, carbon monoxide, and hydrogen sulfide,<sup>19,20</sup> and oxygen partial pressure.<sup>21</sup> The  $\text{Pt}/\text{TiO}_2$  interface is expected to further enhance the sensitivity of  $\text{TiO}_2$  conductivity to

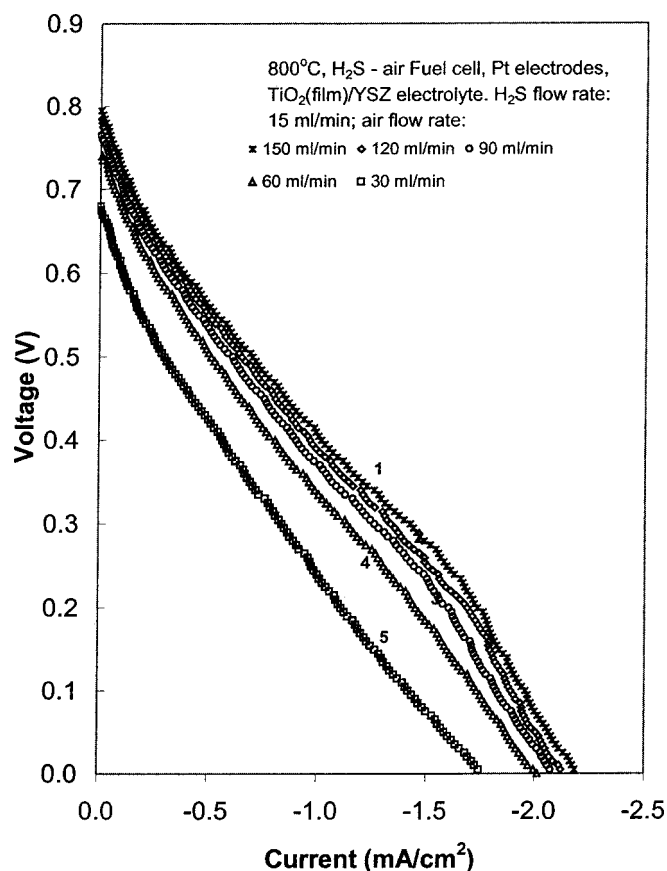


**Figure 10.** Performance of H<sub>2</sub>S fuel cell as a function of air flow rate. H<sub>2</sub>S flow rate, 15 mL/min; air flow rate, 1, 125; 2, 100; 3, 75; 4, 50; and 5, 25 mL/min; *T* 800°C.

reducing conditions due to the spillover. Spillover is characterized by the local separation of the sites of activation and reaction. H<sub>2</sub>S will be activated to form Pt-H species (Eq. 3) which then react with oxide ions (Eq. 5)<sup>22,23</sup>



Since the electrical conductivity of Pt/TiO<sub>2</sub>/YSZ at the anode side is very sensitive to a reducing atmosphere,<sup>22,24-26</sup> injection of electrons into the TiO<sub>2</sub>/YSZ structure from the spatial polaron layer of TiO<sub>2</sub> may increase the electronic conductivity of TiO<sub>2</sub>/YSZ. Therefore, the cell performance will decrease due to the internal electrical loss.

In this test, the spin-coated thin TiO<sub>2</sub> layer applied by the sol-gel technique was very dense and the TiO<sub>2</sub> islands covered most of the YSZ surface, thereby partly blocking the transportation of reactants and products to-and-from the reaction interface, H<sub>2</sub>S/Pt/TiO<sub>2</sub>/YSZ. Therefore, a porous TiO<sub>2</sub> layer was modified by scratching the TiO<sub>2</sub> paste before heat-treatment and then the Pt layer was coated onto the resulting porous TiO<sub>2</sub> layer. Thereby the amount of interface of TiO<sub>2</sub>/YSZ was decreased. The voltage-current performance using this porous TiO<sub>2</sub> layer was improved significantly when compared to the performance using the screen-printed TiO<sub>2</sub> layer, as shown in Fig. 12. The improvement is attributed to the significant increase of the spillover of H<sub>2</sub>S on Pt/TiO<sub>2</sub> during the reaction processes.

The addition of the TiO<sub>2</sub> intermediate layer essentially increased the stability of the H<sub>2</sub>S-O<sub>2</sub> fuel cell. The OCV of the H<sub>2</sub>S-O<sub>2</sub> fuel cell initially decreased over a 1 day operation, then remained stable

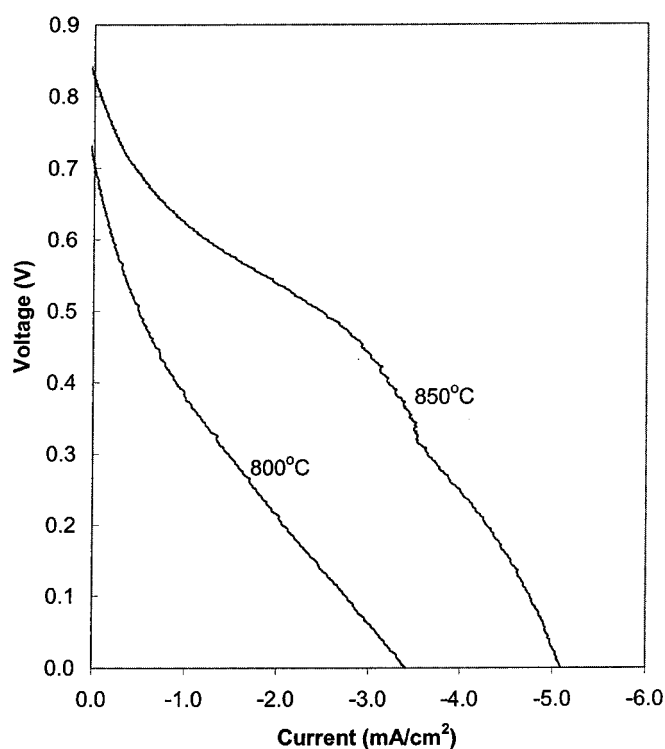


**Figure 11.** Current as a function of voltage for fuel cell: H<sub>2</sub>S, Pt/TiO<sub>2</sub>/YSZ/Pt. Flow rates: H<sub>2</sub>S, 25 mL/min; air, 75 mL/min.

during a subsequent operation for periods of 1 week or longer. The cell was run at 0.4 V for 5 h periods during each measurement, with the shut down of applied potential between tests. Figure 13 gives the plots of OCV and current density at a potential of 0.4 V as a func-

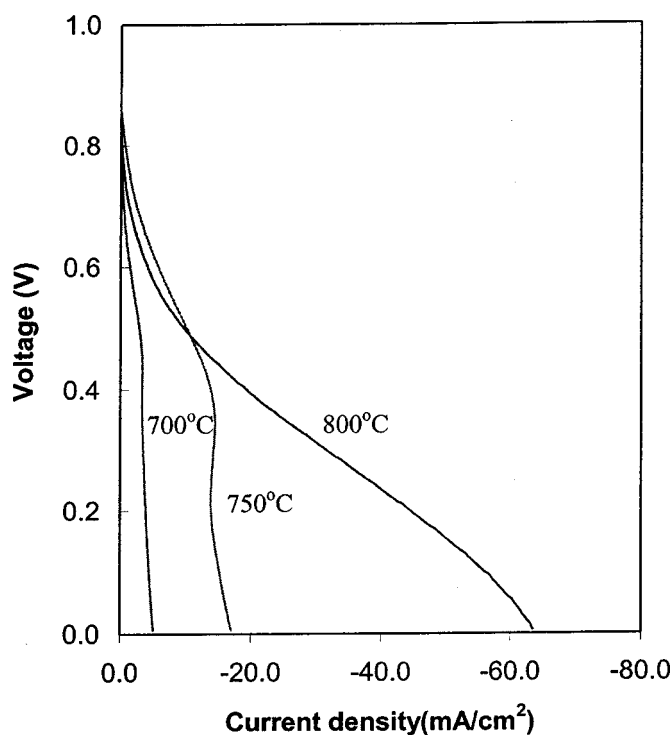


**Figure 12.** Current as a function of voltage for fuel cell: H<sub>2</sub>S, Pt/TiO<sub>2</sub> (paste painting)/YSZ/Pt. Flow rates: H<sub>2</sub>S, 25 mL/min; air, 75 mL/min.

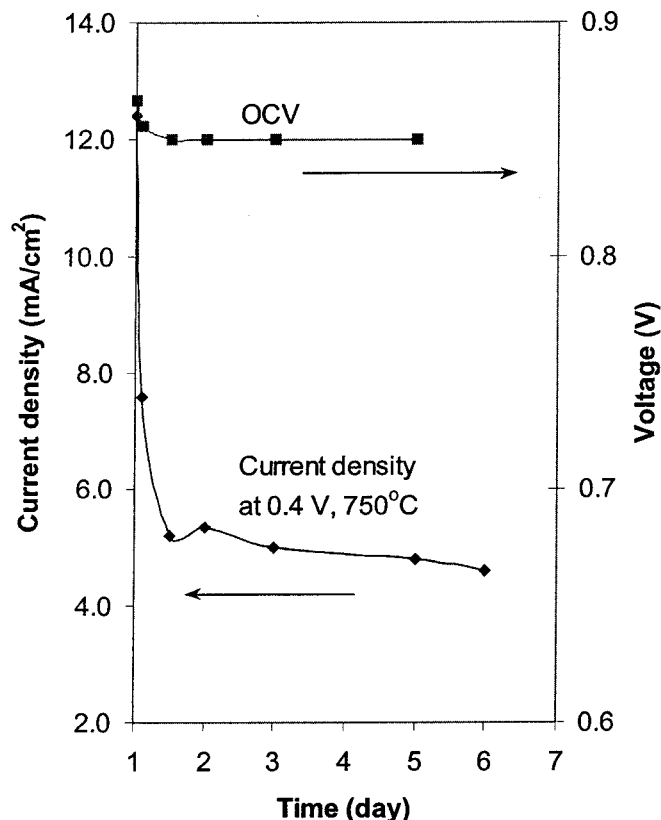


**Figure 13.** Stability of H<sub>2</sub>S fuel cell with TiO<sub>2</sub> interface layer. Flow rates: H<sub>2</sub>S, 15 mL/min; air, 75 mL/min.

tion of time on stream at 750°C. The output current at 0.4 V varied with time on stream in a similar manner to OCV. The decline of the OCV and the current density at the beginning of the operation are attributed to migration of Ti(IV) ions into the YSZ structure, and the consequent increase in the electronic conductivity of YSZ. Since TiO<sub>2</sub> is not a good oxygen ion conductor, the active electrochemical reaction sites in this system were H<sub>2</sub>S/Pt/TiO<sub>2</sub>/YSZ and H<sub>2</sub>S/Pt/YSZ, rather than the interface of Pt/TiO<sub>2</sub>. The interface Pt/TiO<sub>2</sub> is stable during the reaction, which enhances the stability of the system by anchoring the Pt anode onto the YSZ wafer, and thereby preventing detachment.

The good physical and electrical stability of the Pt anode achieved using TiO<sub>2</sub>-modified wafers is a promising result for high-temperature H<sub>2</sub>S fuel cells. H<sub>2</sub>S is an extremely corrosive gas, which poisons the catalysts for H<sub>2</sub>-O<sub>2</sub> fuel cells and has the potential to disrupt catalyst structures. These effects result in short lifetimes of most SOFC H<sub>2</sub>S fuel cells described to date. The improvement in stability of cell performance described above is attributable to stabilization of active reaction sites and securing of the Pt anode catalyst to the YSZ wafer by the TiO<sub>2</sub> layer.

### Conclusions

Platinum anodes deposited on YSZ having an intermediate layer of TiO<sub>2</sub> are more stable than Pt/YSZ anodes for operation in a

H<sub>2</sub>S-O<sub>2</sub> fuel cell. When Pt is directly bonded to YSZ, the Pt/YSZ interface is physically unstable over time in an H<sub>2</sub>S atmosphere and the Pt anode becomes detached. This phenomenon is attributed to reversible formation and decomposition of PtS on the platinum anode interface surface. Contamination of Pt/YSZ electrodes by H<sub>2</sub>S gas is severe at temperatures up to 800°C. At temperatures higher than 850°C, poisoning and fouling of the anode are partly alleviated due to the thermal instability of PtS. PtS can be cleaned from the electrode by polarizing the electrode in an H<sub>2</sub> atmosphere or baking the wafer in a N<sub>2</sub> atmosphere at high temperature. Use of pure H<sub>2</sub>S anode feed does not improve cell performance in the H<sub>2</sub>S fuel cell when compared to 5% H<sub>2</sub>S/N<sub>2</sub> feed. A very thin (submicrometers) layer of TiO<sub>2</sub> added to the anode surface of the YSZ before depositing the Pt anode stabilizes the Pt/YSZ interface. Stability of performance of the platinum anode has thereby been significantly improved by the intermediate layer of TiO<sub>2</sub>, which helps anchor the Pt anode and increases the activity.

### Acknowledgments

This research was supported by Natural Sciences and Engineering Research Council of Canada Strategic Project Grant. We thank T. Barker for the SEM and EDX measurements.

The University of Alberta assisted in meeting the publication costs of this article.

### References

1. N. U. Pujare, K. W. Semkow, and A. F. Sammells, *J. Electrochem. Soc.*, **134**, 2639 (1987).
2. N. U. Pujare, K. J. Tsai, and A. F. Sammells, *J. Electrochem. Soc.*, **136**, 3662 (1989).
3. I. V. Yentekakis and C. G. Vayenas, *J. Electrochem. Soc.*, **136**, 996 (1989).
4. T. J. Kirk and J. Winnick, *J. Electrochem. Soc.*, **140**, 3494 (1993).
5. D. Peterson and J. Winnick, *J. Electrochem. Soc.*, **145**, 1449 (1998).
6. D. Peterson and J. Winnick, *J. Electrochem. Soc.*, **143**, L55 (1996).
7. C. Yates and J. Winnick, *J. Electrochem. Soc.*, **146**, 2841 (1999).
8. U. Kohler and H.-W. Wassmuth, *Surf. Sci.*, **117**, 668 (1982).
9. (a) S. V. Slavov, K. T. Chuang, A. R. Sanger, J. C. Donini, J. Kot, and S. Petrovic, *Int. J. Hydrogen Energy*, **23**, 1203 (1998); (b) K. T. Chuang, J. C. Donini, A. R. Sanger, and S. V. Slavov, *Int. J. Hydrogen Energy*, **25**, 887 (2000).
10. T. W. Kueper, S. J. Visco, and L. C. De Jonghe, *Solid State Ionics*, **52**, 251 (1992).
11. K. Kobayashi, K. Kato, K. Terabe, S. Yamaguchi, and Y. Iguchi, *J. Ceram. Soc. Japan*, **106**, 860 (1998).
12. K. Kordes and G. Simader, in *Fuel Cells and Their Applications*, Chap. 4.6, VCH, New York (1996).
13. S. P. S. Badwal, *Solid State Ionics*, **52**, 23 (1992).
14. Y. Uchimoto, K. Tsutsumi, T. Ioroi, Z. Ogumi, and Z.-I. Takehara, *J. Am. Ceram. Soc.*, **83**, 77 (2000).
15. S. P. S. Badwal and K. Foger, *Mater. Forum*, **21**, 187 (1997).
16. J. Zaman and A. Chakma, *Fuel Process. Technol.*, **41**, 159 (1995).
17. A. Piepu, O. Saur, J. C. Lavalley, O. Legendre, and C. Nede, *Catal. Rev. Sci. Eng.*, **40**, 409 (1998).
18. M. T. Colomer, J. R. Jurado, R. M. C. Marques, and F. M. B. Marques, in *Solid Oxide Fuel Cells*, S. C. Singhal and H. Iwahara, Editors, PV 93-4, p. 523, The Electrochemical Society Proceedings Series, Pennington, NJ (1993).
19. R. M. C. Marques, J. R. Frade, and F. M. B. Marques, in *Solid Oxide Fuel Cells*, S. C. Singhal and H. Iwahara, Editors, PV 93-4, p. 513, The Electrochemical Society Proceedings Series, Pennington, NJ (1993).
20. T. Norby, *Solid State Ionics*, **40/41**, 857 (1990).
21. J. B. Bates, J. C. Wang, and R. A. Perkins, *Phys. Rev. B*, **19**, 4130 (1979).
22. U. Balachandran and N. G. Eror, *J. Mater. Sci.*, **23**, 2676 (1988).
23. U. Roland, R. Salzer, T. Braunschweig, F. Roessner, and H. Winkler, *J. Chem. Soc., Faraday Trans.*, **91**, 1091 (1995).
24. N. M. Rodriguez and R. T. K. Baker, *J. Catal.*, **140**, 287 (1993).
25. K. L. Scholl and E. A. Fletcher, *Energy*, **18**, 69 (1993).
26. J. H. Park and R. N. Blumenthal, *J. Electrochem. Soc.*, **136**, 2867 (1989).